Detailed FD–TD Analysis of Electromagnetic Fields Penetrating Narrow Slots and Lapped Joints in Thick Conducting Screens

ALLEN TAFLOVE, SENIOR MEMBER, IEEE, KORADA R. UMASHANKAR, SENIOR MEMBER, IEEE, BENJAMIN BEKER, STUDENT MEMBER, IEEE, FADY HARFOUSH, STUDENT MEMBER, IEEE, AND KANE S. YEE

Abstract—**The physics of electromagnetic wave transmission through narrow slots and lapped joints in thick conducting screens is examined in detail by applying numerical models to compute both field distributions within the slots and joints, and fields transmitted to the shadow region. The primary modeling tool is the finite-difference time-domain (FD-TD) method, using a Faraday's law contour integral approach to develop new and simple modifications of the basic FD-TD algorithm to properly model the slot physics, even when the slot gap width is much less than one space lattice cell. Finely sampled method of moments (MM) models are used to validate the FD-TD tool for relatively simple straight slots; FD-TD is then used to explore properties of more complicated lapped joints which are widely used for shielding purposes at junctions of metal surfaces. It is found that previously reported slot resonances (screen thicknesses at which exceptionally large transmission of energy may occur) occur in a more general sense for lapped joints as path-length resonances. That is, the total path length along the lapped joint from the front of the screen to the back can become resonant, despite the presence of a number of right-angle turns in the joint path. In addition to greatly enhanced power transmission, path-length resonances can result in total fields within the joint exceeding the incident fields by more than one order of magnitude. Sample field distributions for this case are given. This field enhancement might cause sparking and other nonlinear effects during high-power microwave (HPM) illumination, and must be accounted in HPM coupling studies.**

I. Introduction

RECENT interest in potential defense applications of high-power microwaves (HPM) has added another dimension to the venerable problem of electromagnetic wave coupling through apertures in conducting screens. Essentially, HPM incident power densities can be sufficiently high that nonlinear effects such as air breakdown may occur, especially in regions where electric field enhancements arise. If air breakdown occurs near or within an aperture, it has been hypothesized that the resulting complex effects may not always result in mitigation of the aperture coupling; scenarios have been sketched wherein coupling may, in fact, be enhanced.

Manuscript received April 28, 1986; revised January 29, 1987. This work was supported in part by Lawrence Livermore National Laboratory under Contract 6599805.

A. Taflove and F. Harfoush are with the Department of Electrical Engineering and Computer Science, Technological Institute, Northwestern University, Evanston, IL 60201.

K. R. Umashankar and B. Beker are with the Department of Electrical Engineering and Computer Science, University of Illinois at Chicago, Chicago, IL 60680.

K. S. Yee is with Lockheed Missiles and Space Co., Sunnyvale, CA 94086.

IEEE Log Number 8718304.

The uncertainty of the nonlinear aperture physics, combined with the perception that the development of HPM technology increases the urgency of understanding coupling and shielding, has prompted renewed interest in the basic physics of linear coupling through apertures. In particular, interest has focused on the internal field distributions and coupled power of realistic junctions between metal surfaces, such as lapped joints, wherein efforts are made to attenuate coupling by employing close machining tolerances, gaskets, and other loading.

The first accurate treatment of electromagnetic wave coupling through small holes used the concept of aperture polarizability and was specialized for planar conducting screens of infinite surface area but zero thickness [1]–[3]. As the aperture size increases, or as the screen acquires a finite thickness, the polarizability concept becomes inadequate, and an approach involving generalized admittances is found to be a useful alternative [4]–[8]. Here, the equivalence principle [9, sec. 3-5] is used to divide the original problem into three coupled equivalent problems for the left-hand half-space, the aperture cavity, and the right-hand half-space. Continuity of the tangential components of the E- and H-fields across the boundaries (apertures) between the regions is enforced, yielding operator equations which can be solved using the method of moments (MM) [10]. The fields within the aperture cavity are expanded in terms of transmission line or waveguide modes as appropriate, yielding expressions for the aperture cavity admittance matrix elements which can be directly incorporated into the admittance formulation resulting from the MM procedure. Results for fields in the aperture cavity, and power transmitted through the aperture cavity to the shadow-side half-space region, can then be obtained in a straightforward manner.

The generalized admittance approach [4]–[8] has provided very useful results for transmission through narrow infinitely long slots and electrically small circular holes in large planar screens of finite thickness. Important coupling phenomenology, such as the effects of resonant screen thicknesses and dielectric loading in the aperture cavities, has been deduced by applying this approach to numerous canonical problems.

The goal of this paper is to describe a recently developed alternative to the generalized admittance approach which may permit numerical modeling of even more realistic aperture transmission problems, ultimately including the nonlinear

0018-926X/88/0200-0247$01.00

effects of air breakdown relevant to the HPM shielding problem. This new approach is based upon the finite-difference time-domain (FD-TD) method [11]–[20], using a Faraday's law contour integral approach to develop new and simple modifications of the basic FD-TD algorithm to properly model slot physics, even when the slot gap width is much less than one FD-TD space lattice cell.

After presenting the contour integral approach and resulting FD-TD algorithm modifications, this paper will report validation studies for the new tool. Here, computed data for the magnitude and phase of the fields obtained using FD-TD and a finely sampled MM model are compared for the case of a slot in a planar conducting screen of finite size and thickness subjected to transverse electric (TE) illumination. In the case studied, a simple straight slot, the locus of field comparison is within the slot along the center line between adjacent screen surfaces. The FD-TD model is then used to explore the linear coupling physics of a more complicated U-shaped lapped joint, especially the path-length resonance properties of such a joint. Ongoing work, to be described in a subsequent paper, applies the FD-TD tool to similar apertures in the walls of three-dimensional cavities with validation by experiment, similar to the hybrid FD-TD multiconductor coupling model recently described [24].

II. Background of the Basic FD–TD Method

In the mid-1960's, Yee introduced a computationally efficient means of directly solving Maxwell's time-dependent curl equations using finite differences [11]. With this approach, the continuous electromagnetic field in a finite volume of space is sampled at distinct points in a space lattice and at distinct equal-spaced points in time. Wave propagation, scattering, and penetration phenomena are modeled in a self-consistent manner by marching in time, that is, repeatedly implementing the finite-difference analog of the curl equations at each lattice point. This results in a simulation of the continuous actual waves by sampled-data numerical analogs propagating in a data space stored in a computer. Space and time sampling increments are selected to avoid aliasing of the continuous field distribution and to guarantee stability of the time-marching algorithm [12]. Time marching is completed when the desired late-time or sinusoidal steady-state field behavior is observed.

The Yee formulation, designated as the finite-difference time-domain method, permits in principle the modeling of electromagnetic wave interactions with a level of detail comparable to that of the method of moments. Further, the explicit nature of the Yee algorithm leads to overall computer storage and running time requirements for FD-TD that are linearly proportional to N, the number of field unknowns in the finite volume of space being modeled.[1] These two attributes indicated promise for FD-TD in enabling detailed numerical models of wave interactions with structures having volumetric complexity, such as biological tissues [13] and loaded cavities [14], [15]. The direct time-domain nature of FD-TD also indicated promise for detailed modeling of electromagnetic pulse (EMP) interactions with complex structures [16]–[18].

However, the use of FD-TD was very limited until the early 1980's because of a number of basic problems. First, Yee's formulation provided for no simulation of the field sampling space extending to infinity. This deficiency caused spurious nonphysical reflection of the numerical wave analogs at the outermost planes of the space lattice. Second, it provided for no simulation of an incident wave having an arbitrary duration, angle of incidence, or angle of polarization. Third, it provided for no means to obtain unambiguous sinusoidal steady-state magnitude and phase data directly from the computed transient field response. Fourth, it provided for no means to simulate wave interactions with important structures, such as wires and slots, having dimensions smaller than one lattice cell. Fifth, it provided for no means to compute far-field radiation or scattering patterns. Sixth, its required volumetric space discretization caused its computer resource needs to seem prohibitive.

By the mid-1980's, the major difficulties with FD-TD were largely overcome. Building on basic research in one-way wave equations and high-order expansions for radiation conditions [19], a numerical radiation boundary condition was formulated [20] which accurately simulates the extension of the FD-TD field sampling space to infinity. An accurate simulation of an incident wave of arbitrary duration, pulse shape, angle of incidence, and angle of polarization was reported independently in [20] and [21]. This was accomplished by zoning the FD-TD space lattice into a total-field region (in which the structure of interest is embedded) surrounded by a scattered-field region, and providing a proper connecting condition between the regions. Additional work provided means to obtain unambiguous sinusoidal steady-state data from the transient response [21], [22], to accurately compute far scattered fields and monostatic/bistatic radar cross section [21]–[23]; to accurately compute coupling to wires and wire bundles in free space and in a metal cavity [24], [25]; and to achieve conformal models of smoothly curved target surfaces without staircasing [26]. Finally, evolving computer hardware and software technology provided means to satisfy FD-TD requirements in central memory size, arithmetic speed, and bandwidth to high-speed secondary memory to enable routine usage of FD-TD for modeling three-dimensional structures containing more than 10^6 unknown electromagnetic field components in less than 5 min per illumination angle [25].

III. Contour Integral Interpretation

A. Rationale

The Yee algorithm for FD-TD was originally interpreted as a direct approximation of the pointwise derivatives of Maxwell's time-dependent curl equations using numerical central differences [11]. Although this interpretation is useful for understanding how FD-TD models wave propagation away from material surfaces, it sheds little light on what algorithm modifications are needed to model the physics of fine geometrical features properly, such as wires, slots, and curved

[1] For nonresonant structures spanning approximately 0.1 to 30 wavelengths.

surfaces requiring subcell spatial resolution. Modeling of such features has become increasingly important as confidence in the basic predictive powers of FD-TD has grown.

Recent work has indicated that extension of FD-TD modeling to wires, slots, and curved surfaces can be achieved by departing from Yee's original pointwise derivative interpretation. As shown in Fig. 1, the new idea involves starting with a more macroscopic (but still local) combined-field description based upon Ampere's law and Faraday's law in *integral* form, implemented on an array of electrically small spatially orthogonal contours. These contours mesh (intersect) in the manner of links in a chain, providing a geometrical interpretation of the coupling of Ampere's law and Faraday's law. This meshing results in the filling of the FD-TD modeled space by a three-dimensional chain-link array of intersecting orthogonal contours. The presence of wires, slots, and curved surfaces can be accounted by incorporating appropriate field behavior into the contour and surface integrals implementing Ampere's law and Faraday's law at selected meshes, and by deforming contour paths as required to conform with surface curvature.

B. Equivalence to the Yee Algorithm in Free Space

We shall first demonstrate the equivalence of the Yee and contour integral interpretations for the free-space case. For simplicity, FD-TD expressions will be developed for only one field component in Fig. 1(a) and one field component in Fig. 1(b); extension to all of the rest will be seen to be straightforward.

Applying Ampere's law along contour C_1 in Fig. 1(a), and assuming that the field value at a midpoint of one side of the contour equals the average value of that field component along that side, we obtain

$$\frac{\partial}{\partial t}\int_{S_1}\mathbf{D}\cdot\mathbf{dS_1}=\oint_{C_1}\mathbf{H}\cdot\mathbf{dl_1} \tag{1a}$$

$$\begin{aligned}&\frac{\partial}{\partial t}\int_{S_1}\epsilon_0 E_z(i,j,k)\,dS_1\\&=H_x\left(i,j-\frac{1}{2},k\right)\Delta x+H_y\left(i+\frac{1}{2},j,k\right)\Delta y\\&\quad-H_x\left(i,j+\frac{1}{2},k\right)\Delta x-H_y\left(i-\frac{1}{2},j,k\right)\Delta y.\end{aligned} \tag{1b}$$

Now, further assuming that $E_z(i, j, k)$ equals the average value of E_z over the surface S_1; that $\Delta x = \Delta y = \delta$; and that the time derivative can be numerically realized using a central-difference expression, (1b) reduces to

$$\begin{aligned}&\epsilon_0\delta^2\cdot\left[\frac{E_z^{n+1}(i,j,k)-E_z^n(i,j,k)}{\delta t}\right]\\&=\left[H_x^{n+(1/2)}\left(i,j-\frac{1}{2},k\right)-H_x^{n+(1/2)}\left(i,j+\frac{1}{2},k\right)\right.\\&\quad\left.+H_y^{n+(1/2)}\left(i+\frac{1}{2},j,k\right)-H_y^{n+(1/2)}\left(i-\frac{1}{2},j,k\right)\right]\cdot\delta\end{aligned} \tag{1c}$$

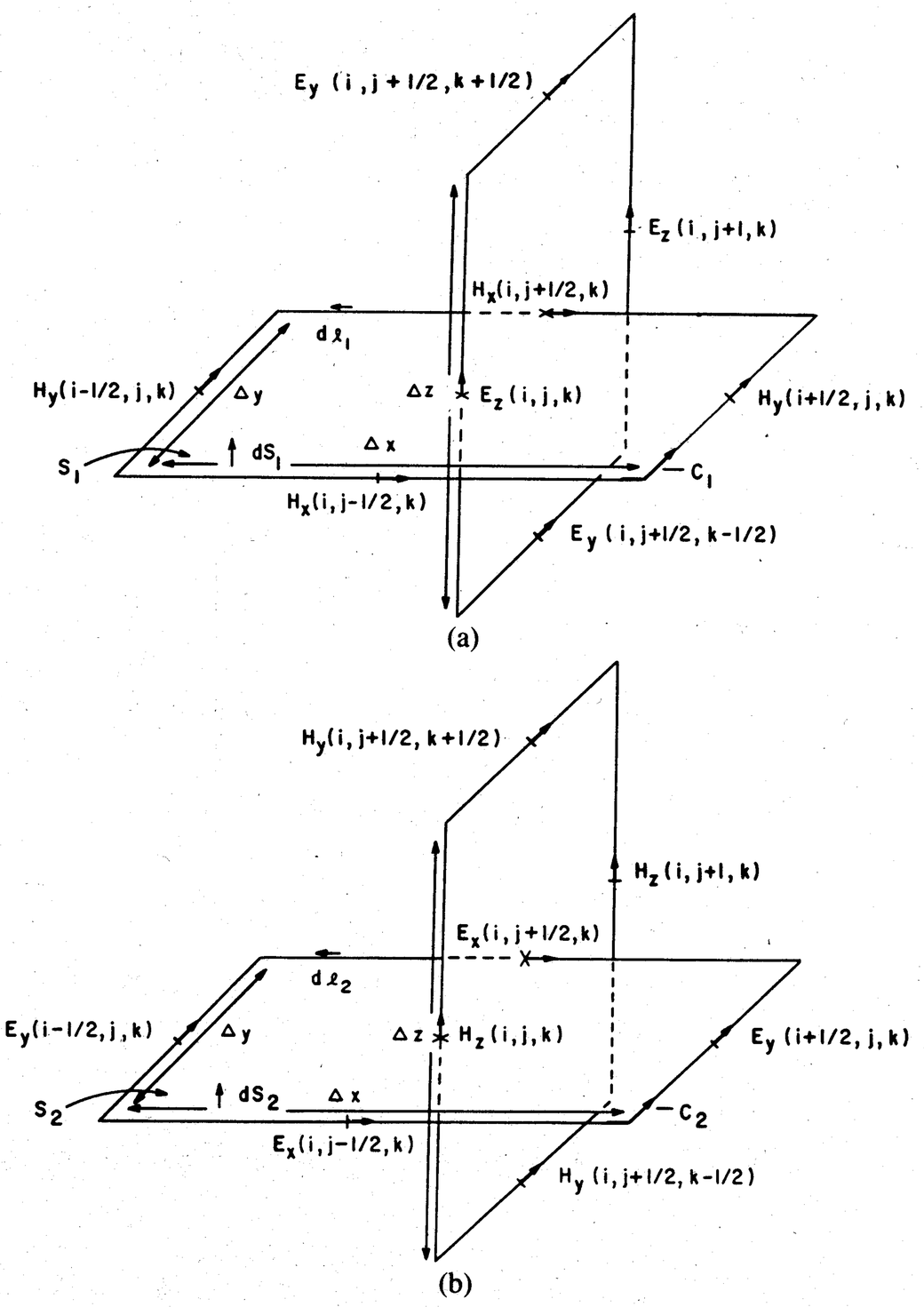

Fig. 1. Examples of spatially orthogonal contours in free space. (a) Ampere's law for E_z. (b) Faraday's law for H_z.

where the superscripts indicate field values at time steps n, $n + (1/2)$, and $n + 1$. Isolation of $E_z^{n+1}(i, j, k)$ on the left side then yields exactly the Yee time-stepping expression for E_z for the free-space case that was obtained directly from implementing the curl H equation with finite differences.

In an analogous manner, we can apply Faraday's law along contour C_2 in Fig. 1(b), obtaining

$$\frac{\partial}{\partial t}\int_{S_2}\mathbf{B}\cdot\mathbf{dS_2}=-\oint_{C_2}\mathbf{E}\cdot\mathbf{dl_2} \tag{2a}$$

$$\begin{aligned}&\frac{\partial}{\partial t}\int_{S_2}\mu_0 H_z(i,j,k)\,dS_2\\&=-E_x\left(i,j-\frac{1}{2},k\right)\Delta x-E_y\left(i+\frac{1}{2},j,k\right)\Delta y\\&\quad+E_x\left(i,j+\frac{1}{2},k\right)\Delta x+E_y\left(i-\frac{1}{2},j,k\right)\Delta y\end{aligned} \tag{2b}$$

$$\begin{aligned}&\mu_0\delta^2\cdot\left[\frac{H_z^{n+(1/2)}(i,j,k)-H_z^{-(1/2)}(i,j,k)}{\delta t}\right]\\&=\left[E_x^n\left(i,j+\frac{1}{2},k\right)-E_x^n\left(i,j-\frac{1}{2},k\right)\right.\\&\quad\left.+E_y\left(i-\frac{1}{2},j,k\right)-E_y\left(i+\frac{1}{2},j,k\right)\right]\cdot\delta.\end{aligned} \tag{2c}$$

Isolation of $H_z^{n+(1/2)}(i, j, k)$ on the left side yields exactly the Yee time-stepping expression for H_z for the free-space case that was obtained directly from implementing the curl E equation with finite differences.

C. Application to the Thin Wire

To illustrate how the contour integral interpretation permits incorporation of near-field physics (yielding special-purpose time-stepping expressions that were *not* obvious from the previous pure finite-difference perspective), we shall next consider the case of transverse magnetic (TM) coupling to a thin wire. Fig. 2 illustrates the Faraday's law contour path used to derive the special FD-TD algorithm for the circumferential magnetic fields immediately adjacent to the wire. Although only H_y is shown, the analysis is easily generalized for the other looping magnetic field components.

The following briefly summarizes the assumptions concerning the near-field physics that are incorporated into the Faraday's law model. First, the near scattered circumferential magnetic field components and the near scattered radial electric field components are assumed to vary as $1/r$ near the wire, where r is the distance from the wire center. With r constrained to be less than 0.1 wavelength at any point in C (by FD-TD spatial resolution requirements), the $1/r$ singularity behavior of the scattered H_y and E_x fields is assumed to dominate the respective incident fields so that the total H_y and E_x fields also take on the $1/r$ singularity. Finally, the near total H_y and the near total E_z fields, evaluated at the z midpoint of the contour, are assumed to represent the average values of their respective fields over the full z interval. These assumptions can be concisely summarized by the following expressions, assumed to apply on and within contour C of Fig. 2:

$$H_y(x, z) \simeq H_y\left(\frac{\delta}{2}, z_0\right) \cdot \frac{\left(\frac{\delta}{2}\right)}{x} \cdot [1 + c_1 \cdot (z - z_0)] \quad (3a)$$

$$E_x\left(x, z_0 \pm \frac{\delta}{2}\right) \simeq E_x\left(\frac{\delta}{2}, z_0 \pm \frac{\delta}{2}\right) \cdot \frac{\left(\frac{\delta}{2}\right)}{x} \quad (3b)$$

$$E_z(0, z) = 0 \quad (3c)$$

$$E_z(\delta, z) \simeq E_z(\delta, z_0) \cdot [1 + c_2 \cdot (z - z_0)] \quad (3d)$$

where c_1 and c_2 are arbitrary constants that need not be known.

Using the field expressions of (3a)–(3d), we can now apply Faraday's law of (2a) along contour C. We find that the $1/x$ variations in H_y and E_x yield natural logarithms. Further, the linear odd symmetry variation in z assumed for H_y and E_z integrates out. This yields the following expression:

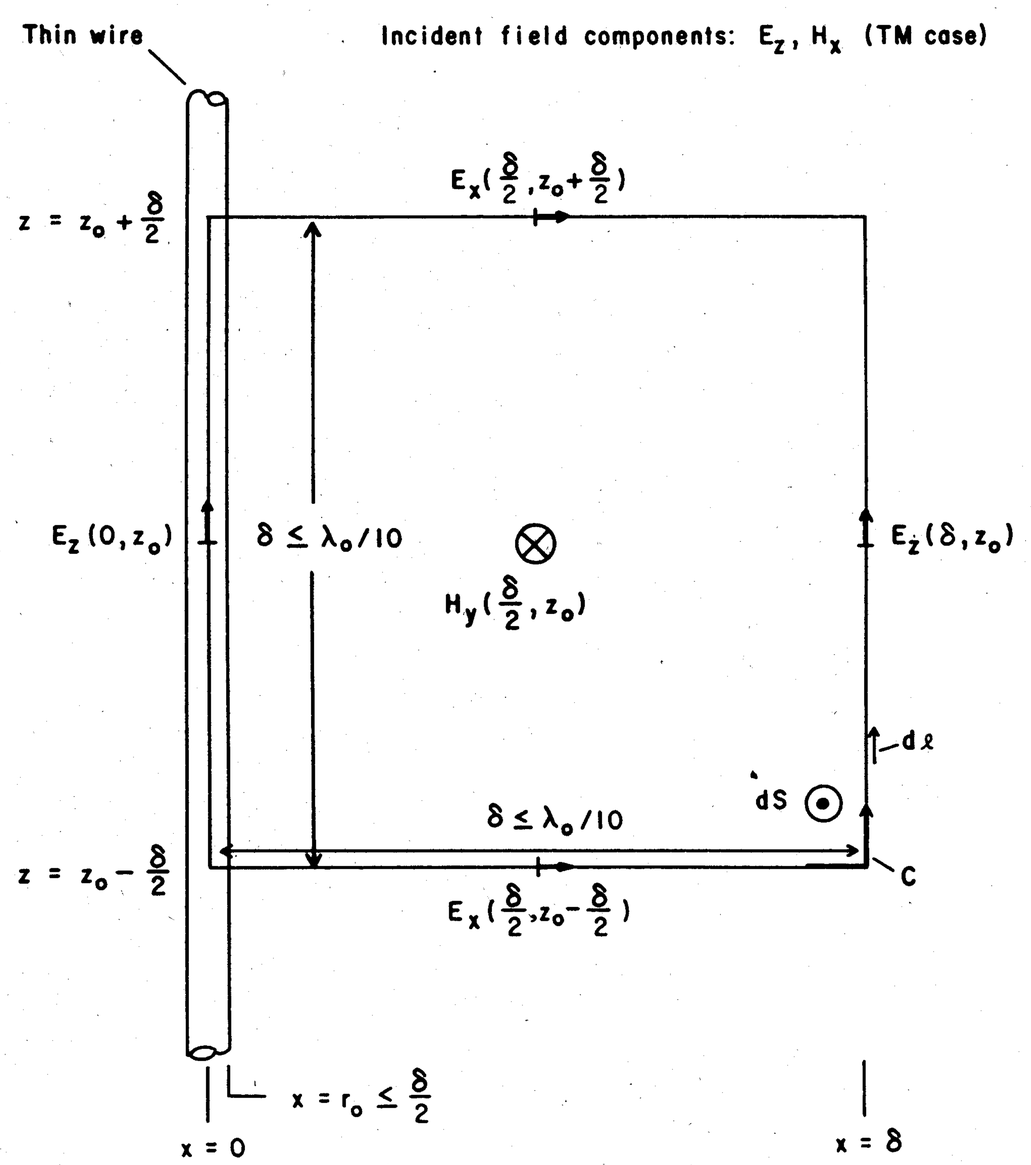

Fig. 2. Faraday's law contour path for thin-wire model.

where r_0 (assumed to be less than 0.5δ) is the wire radius. Isolation of $H_y^{n+(1/2)}(\delta/2, z_0)$ on the left side of (4) yields the required modified time-stepping relation. As stated, the analysis is easily generalized to obtain similar time-stepping relations for the other circumferential magnetic field components immediately adjacent to the wire. Note that *no* other magnetic or electric field components in the FD-TD space lattice require modified time-stepping relations. All other field components are time-stepped using the ordinary free-space Yee algorithm of [11].

The accuracy of this contour integral FD-TD model is demonstrated in Figs. 3 and 4. Fig. 3 compares the FD-TD and eigenfunction expansion solutions for the circumferential magnetic field near a thin perfectly conducting infinitely long wire for the TM two-dimensional case. The FD-TD grid cell size is fixed at 1/10 wavelength, while the wire radius spans a three order of magnitude range from 1/30 000 wavelength (1/3000 cell) to 1/30 wavelength (1/3 cell).[2] The field comparison point is fixed at a distance of 1/20 wavelength (1/2 cell) from the wire center. An excellent agreement within two percent is observed between the FD-TD and eigenfunction expansion solutions over the entire range of wire radius.

Fig. 4 compares the FD-TD and MM solutions for the circumferential magnetic field near a thin perfectly conducting 2.0-wavelength long wire for the TM three-dimensional case.

$$\frac{H_y^{n+(1/2)}\left(\frac{\delta}{2}, z_0\right) - H_y^{n-(1/2)}\left(\frac{\delta}{2}, z_0\right)}{\delta t} \simeq \frac{\left[E_x^n\left(\frac{\delta}{2}, z_0 - \frac{\delta}{2}\right) - E_x^n\left(\frac{\delta}{2}, z_0 + \frac{\delta}{2}\right)\right] \cdot \frac{1}{2} \ln\left(\frac{\delta}{r_0}\right) + E_z^n(\delta, z_0)}{\mu_0 \frac{\delta}{2} \ln\left(\frac{\delta}{r_0}\right)} \quad (4)$$

[2] 15 × 30 cell grid size (using symmetry), requiring 0.6 s of Cray-2 time.

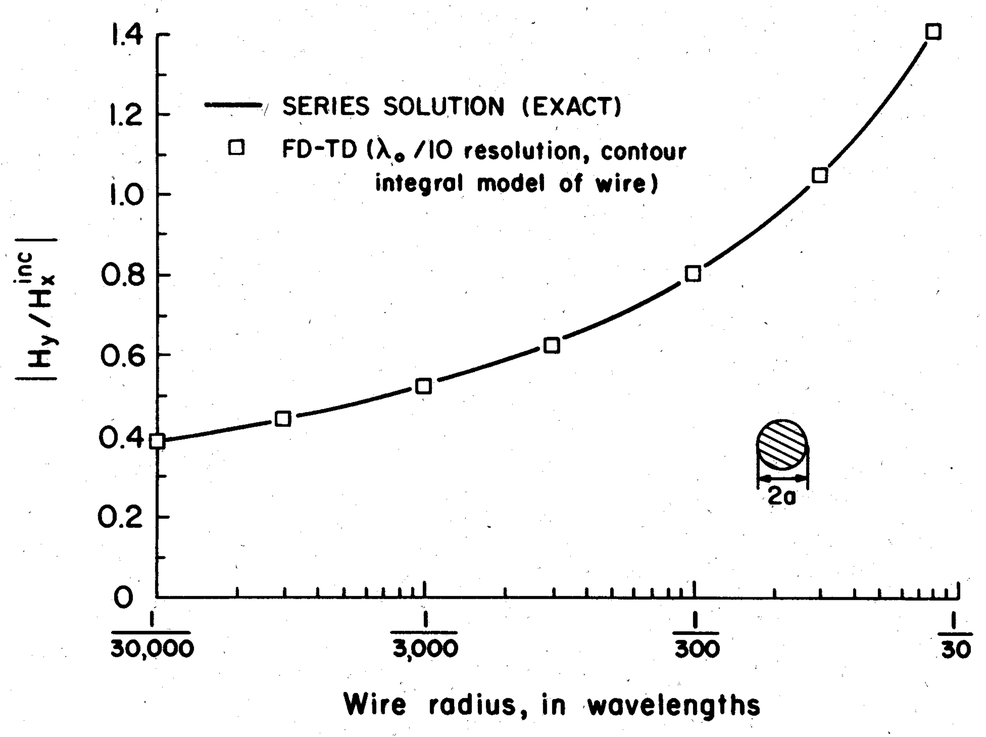

Fig. 3. Comparison of FD-TD and eigenfunction expansion solutions for scattered circumferential magnetic field at point 1/20 wavelength from center of infinite wire.

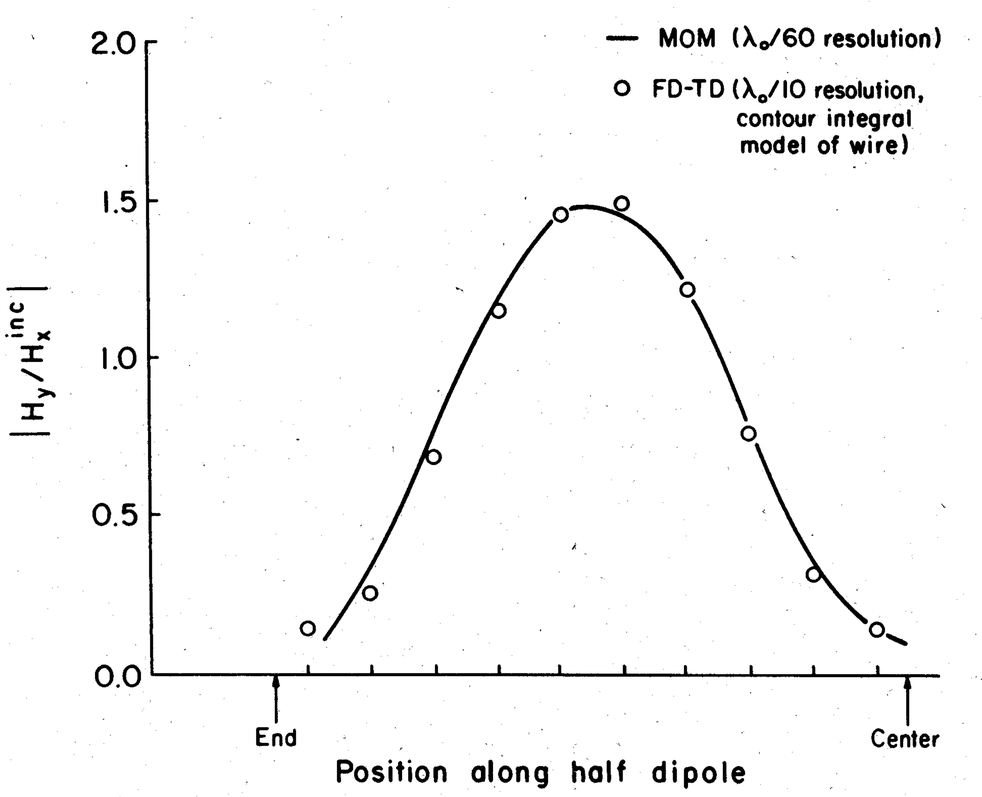

Fig. 4. Comparison of FD-TD and MM solutions for scattered circumferential magnetic field distribution along 2.0-wavelength (antiresonant) wire of radius 1/300 wavelength (broadside TM illumination).

Here, the FD-TD lattice cell size is again 1/10 wavelength, but the wire radius is fixed at 1/300 wavelength (1/30 cell).[3] The MM sampling resolution along the wire is 1/60 wavelength, and the FD-TD/MM field comparison is made along the half-length of the wire (from one end to the center) at a fixed radial distance of 1/20 wavelength (1/2 cell) from the wire center. Excellent agreement is noted despite the fact that the wire length is antiresonant, and the FD-TD model required up to 30 cycles of the incident wave to settle into the sinusoidal steady state.

The approach just described has been recently used as the basis of a hybrid FD-TD/MM technique for modeling coupling to multiconductor wire bundles in free space or metal cavities. See [24] for the details of the hybrid formulation and its validation.

D. Application to the Thin-Slot, Two-Dimensional TE Case

The contour integral interpretation will now be applied to FD-TD modeling of a canonical problem at the focus of the present paper, namely, the thin slot in a planar perfectly conducting screen of finite size and thickness subjected to TE illumination. Fig. 5 illustrates the canonical slot geometry studied here and the Faraday's law contour paths C_1, C_2, and C_3 used to derive special FD-TD algorithms for the longitudinal magnetic field components H_z located immediately adjacent to the screen.

The following briefly summarizes the assumptions concerning the near-field physics that are incorporated into the Faraday's law models of Fig. 5. First, for contour C_1 (away from the slot), field components H_z and E_y are assumed to have no variation in the y direction (perpendicular to the screen). Evaluated at the x midpoint of contour C_1, H_z and E_x are assumed to represent the average values of their respective fields over the full x interval. At contour C_2 (at the opening of the slot), H_z is assumed to represent the average value of the magnetic field over the entirety of the free-space part of S_2. Here, E_y is again assumed to have no variation in the y direction, and E_x is again assumed to represent the average value over the full x interval. At contour C_3 (within the slot), H_z is assumed to represent the average value of the magnetic field over the full y interval, and H_z and E_x are assumed to

[3] 15 × 30 × 20 cell lattice size (using symmetry), requiring 24 s of Cray-2 time.

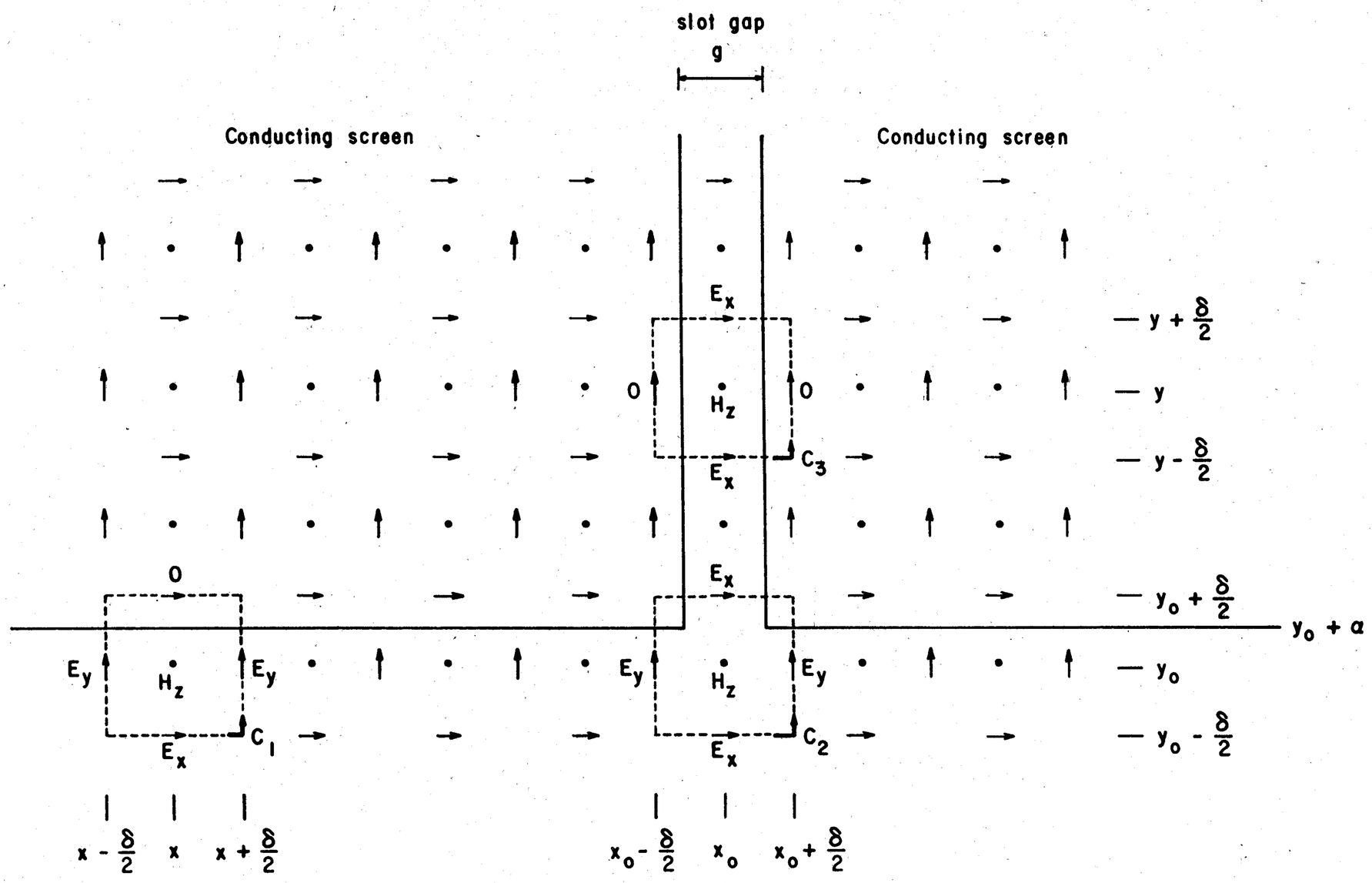

Fig. 5. Faraday's law contour paths for two-dimensional planar conducting screen with thin straight slot (TE case).

have no variation in the x direction (across the slot gap). Finally, for C_1, C_2, and C_3, the portions of the contours located within the conducting screen are assumed to have zero electric and magnetic fields.

After applying Faraday's law of (2a) for the three contours, subject to the foregoing assumptions, the following special FD-TD time-stepping relations are obtained for the H_z components immediately adjacent to the screen.

Away from the slot (contour C_1):

$$\frac{H_z^{n+(1/2)}(x, y_0) - H_z^{n-(1/2)}(x, y_0)}{\delta t} \simeq \frac{\left[E_y^n\left(x-\frac{\delta}{2}, y_0\right) - E_y^n\left(x+\frac{\delta}{2}, y_0\right)\right] \cdot \left(\frac{\delta}{2}+\alpha\right) - E_x^n\left(x, y_0-\frac{\delta}{2}\right) \cdot \delta}{\mu_0 \delta \left(\frac{\delta}{2}+\alpha\right)}. \quad (5a)$$

At the opening (aperture) of the slot (contour C_2):

$$\frac{H_z^{n+(1/2)}(x_0, y_0) - H_z^{n-(1/2)}(x_0, y_0)}{\delta t} \simeq \frac{E_x^n\left(x_0, y_0+\frac{\delta}{2}\right) \cdot g - E_x^n\left(x_0, y_0-\frac{\delta}{2}\right) \cdot \delta + \left[E_y^n\left(x_0-\frac{\delta}{2}, y_0\right) - E_y^n\left(x_0+\frac{\delta}{2}, y_0\right)\right] \cdot \left(\frac{\delta}{2}+\alpha\right)}{\mu_0 \cdot \left[\delta\left(\frac{\delta}{2}+\alpha\right) + g\left(\frac{\delta}{2}-\alpha\right)\right]}. \quad (5b)$$

Within the slot (contour C_3):

$$\frac{H_z^{n+(1/2)}(x_0, y) - H_z^{n-(1/2)}(x_0, y)}{\delta t} \simeq \frac{E_x^n\left(x_0, y+\frac{\delta}{2}\right) \cdot g - E_x^n\left(x_0, y-\frac{\delta}{2}\right) \cdot g}{\mu_0 g \delta}. \quad (5c)$$

In (5c), we note that the slot gap distance g cancels on the right side, reducing the time-stepping relation for H_z in the slot to that of a one-dimensional wave ($\pm y$-directed) in free space. For completeness, we also note that no magnetic or electric field components in the FD-TD space grid, other than the H_z components immediately adjacent to the screen, require modified time-stepping relations.

The accuracy of this contour integral model implemented on a relatively coarse FD-TD grid (having 1/10 wavelength cell size) is now demonstrated by direct comparison of the

computed fields within a thin slot in a conducting screen against high-resolution numerical benchmarks. The screen is assumed to be 1/10-wavelength thick, extending 1/2 wavelength to each side of a slot which has a gap distance g of 1/40 wavelength. Broadside TE illumination is assumed. Three types of predictive data are compared: 1) the low-resolution FD-TD model using the contour integral approach to treat the slot as a 1/4-cell gap;[4] 2) a high-resolution FD-TD model (having 1/40 wavelength cell size) to treat the slot as a 1-cell gap;[5] and 3) a high-resolution MM model (having 1/400-wavelength sampling in the slot and 1/220-wavelength sampling along the screen). Note that unlike the MM models used in the generalized admittance approach [4]–[8], the MM model used here incorporated no *a priori* assumptions concerning transmission line behavior in the slot and, in fact, treated the slotted screen as a pure scattering geometry.

Figs. 6 and 7 graph the magnitude and phase distributions of the gap electric field E_x and magnetic field H_z along an observation line that is perpendicular to the screen and centered in the slot gap. Fig. 8 graphs the variation of the remaining component E_y along a line that is parallel to the first observation line but shifted 1/20 wavelength to one side of the slot center line (since $E_y = 0$ along the exact center of the slot by symmetry). These figures indicate an excellent agreement between all three sets of predictive data, in both magnitude and phase. Of particular interest is the ability of the low-resolution FD-TD model, using the contour integral approach, to compute accurately the peak electric field in the slot. As stated earlier, electric field enhancement of the type seen here may be important in causing nonlinear aperture effects under HPM exposure conditions.

Fig. 9 shows the results of a further investigation in which the slot gap distance g is varied downward from 1/10 wavelength without changing any other features of the screen geometry. Here, the goal is to develop an understanding of gap electric field enhancement in the limit as g approaches zero. The high-resolution MM data at each slot gap width are shown as a vertical bar, and the low-resolution FD-TD (contour integral model) data for the gap field form the solid curve. Good agreement is noted for gap distances dropping from 1/10 wavelength (1 cell) to 1/120 wavelength (1/12 cell). For even narrower slots the FD-TD results continue a smooth trend upward, approaching the value 3.8 at $g = 0$. High-resolution MM data for slots narrower than 1/120 wavelength were not obtained because of numerical instability problems with the MM code observed beyond this point.

IV. Lapped Joints, Two-Dimensional TE Case

Validation and phenomenological studies have been conducted for the contour path FD-TD technique applied to model TE coupling through lapped joints in conducting screens. Of particular interest here was the possibility of resonant transmission effects. This phenomenon was previously reported for straight slots in planar conducting screens of infinite surface area but finite thickness [4]–[8], wherein certain screen thicknesses (approximately an integer multiple of one-half

[4] 30 × 20 cell grid size (using no symmetry), requiring 0.3 s Cray-2 time.
[5] 80 × 40 cell grid size (using no symmetry), requiring 7.0 s Cray-2 time.

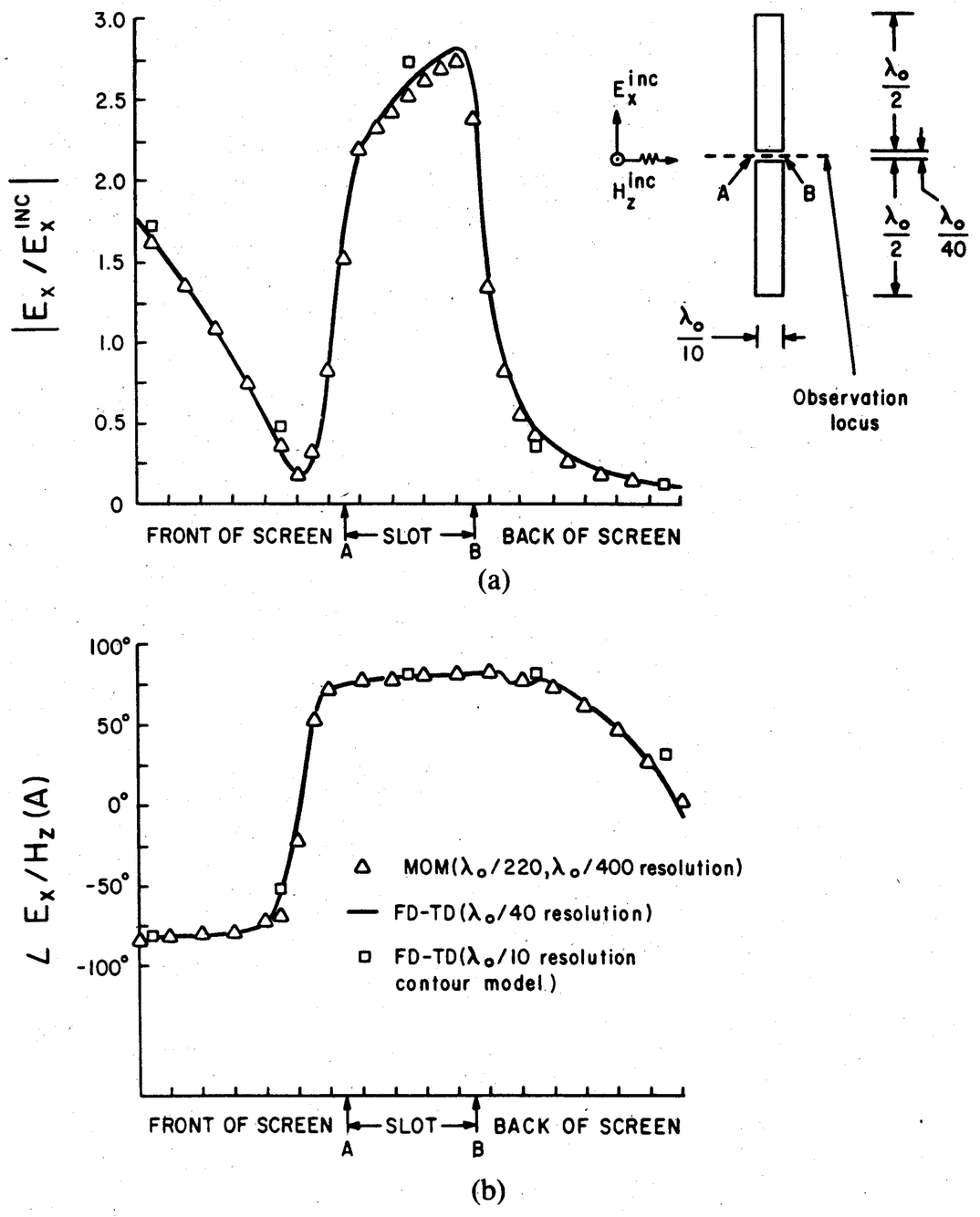

Fig. 6. Comparison of FD-TD and MM solutions for gap electric field distribution, straight-slot case. (a) Magnitude. (b) Phase.

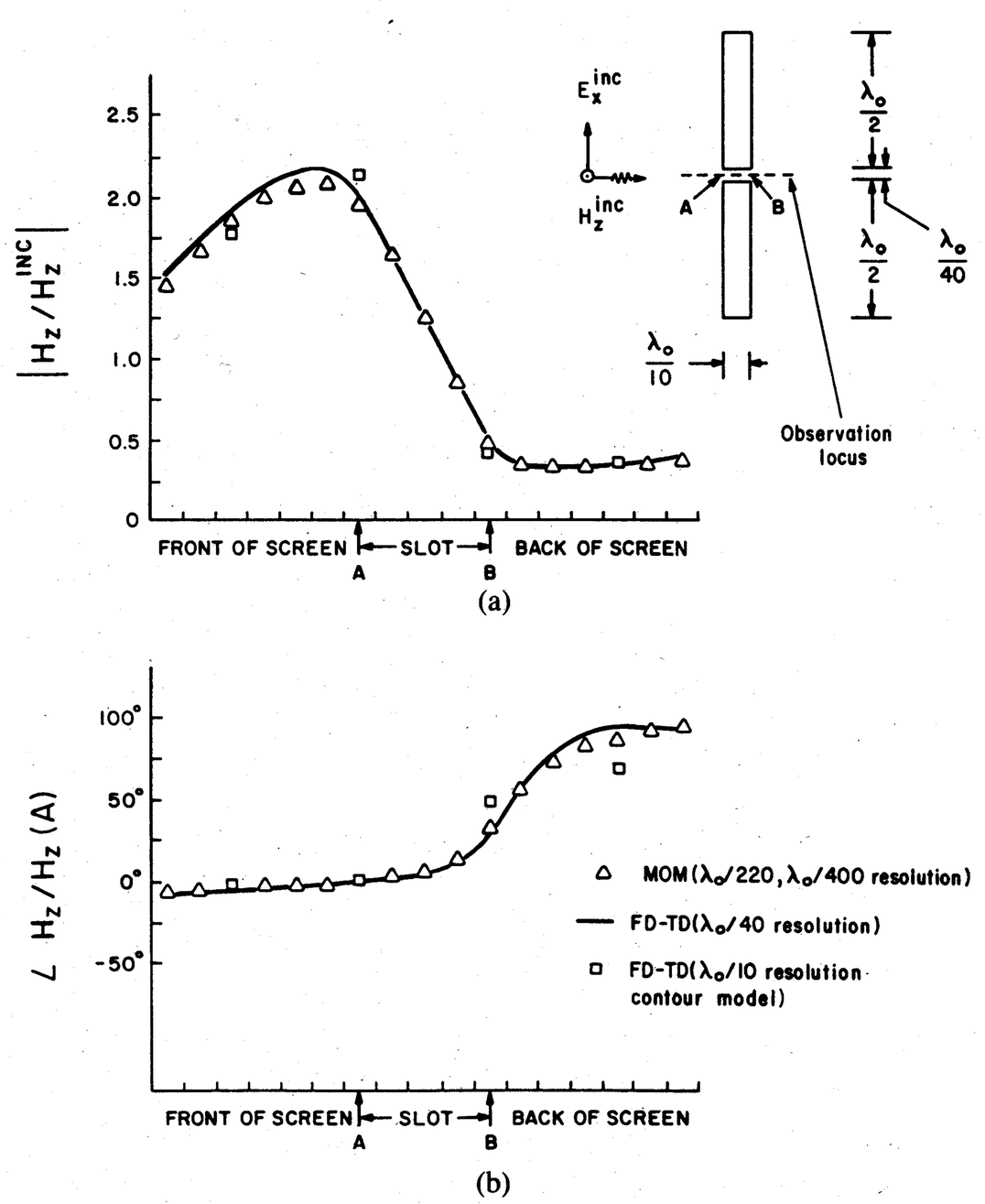

Fig. 7. Comparison of FD-TD and MM solutions for gap magnetic field distribution, straight-slot case. (a) Magnitude. (b) Phase.

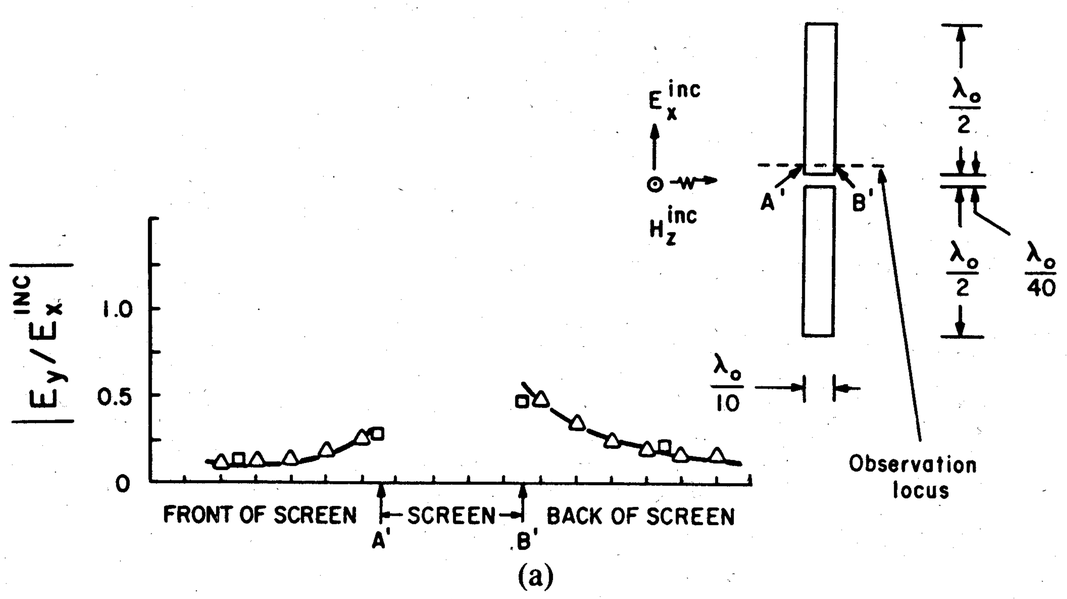

Fig. 8. Comparison of FD-TD and MM solutions for electric field perpendicular to screen, near slot. (a) Magnitude. (b) Phase.

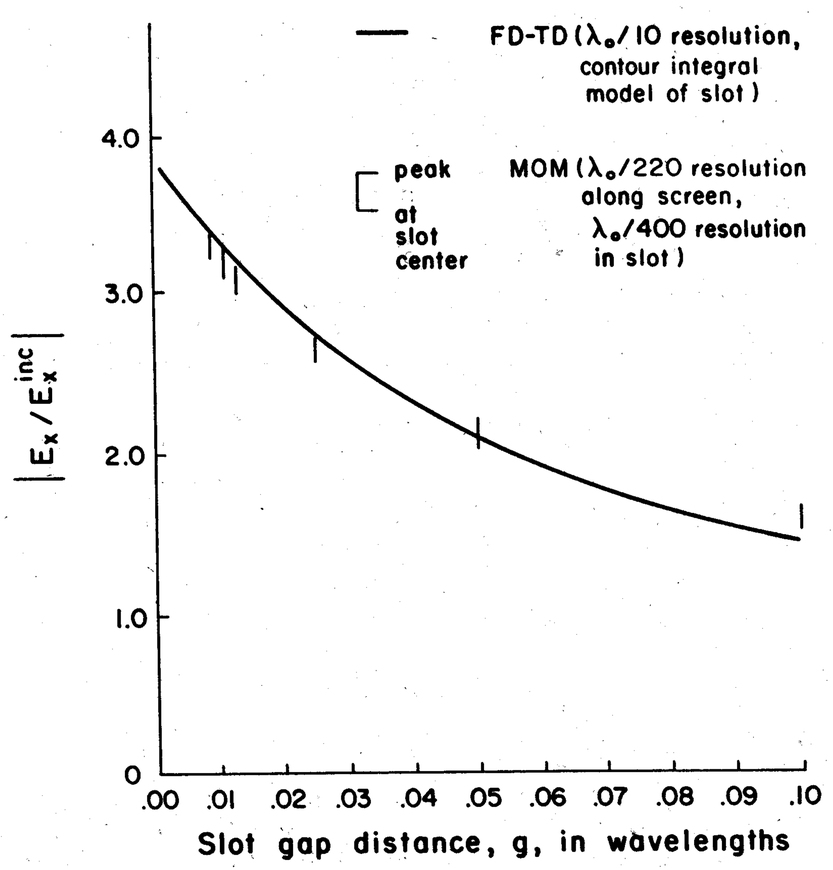

Fig. 9. Comparison of FD-TD contour model and MM calculations for variation of gap electric field with gap distance, straight-slot case.

wavelength) would cause an exceptionally large transmission of energy through a slot. It was conjectured that such resonances could occur in a more general sense for lapped joints as path-length resonances. That is, the total path length through a lapped joint from the front of the screen to the back could become resonant, despite the presence of a number of sharply angled turns in the joint path. This phenomenon in turn might be further generalized to threaded (screw-type) joints.

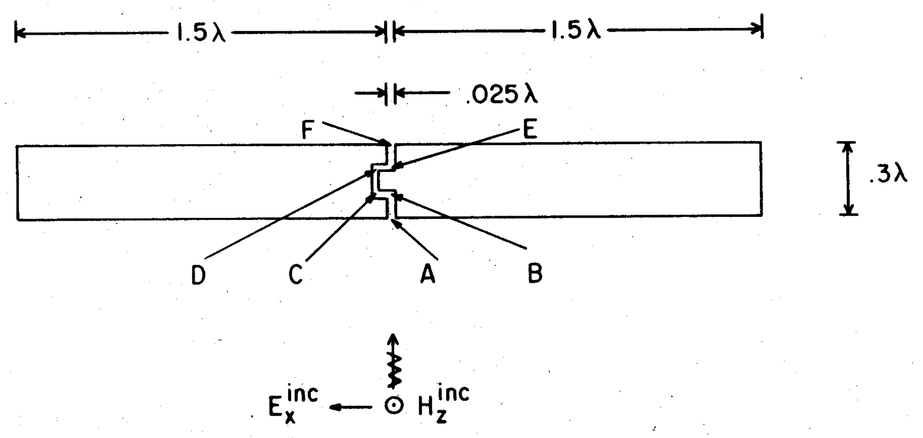

Fig. 10. Geometry of U-shaped lapped joint for TE illumination, shown to scale.

Such joints are widely implemented in practice for microwave shielding and are of importance in HPM studies.

Fig. 10 shows the geometry of a U-shaped lapped joint which was selected for detailed study. The U shape of the joint permits adjustment of the overall joint path length without disturbing the positions of the input and output ports at *A* and *F*. This adjustment can be performed simply by varying path segments *BC* and *DE* from zero to some maximum value set by the screen half-width. In this manner, adjustment of the path length can be performed independently of any other aspect of the scattering problem, so that computed variations of gap fields and power transmission as the path length is varied can be uniquely attributed to that variation.

The joint of Fig. 10, having a uniform gap of 1/40 wavelength, is positioned so that the input and output ports at *A* and *F* are symmetrically located in a conducting screen 3/10 wavelength thick and approximately 3 wavelengths wide. This shield width is selected to obtain a deep shadow region (in the absence of the lapped joint) so that computed fields and power near point *F* are due almost entirely to the actions of the joint.

Fig. 11 presents a study of the equivalent transmission cross section of the lapped joint of Fig. 10 as the total path length, *ABCDEF*, through the joint is varied in distinct 0.05-wavelength steps from 0.3 wavelengths to 1.5 wavelengths. Data for this study result from a high-resolution FD-TD model (having 1/40 wavelength cell size) which treats the joint gap as one full cell.[6] The transmission cross section is defined here as the number of 1/40-wavelength cells that, subjected to the incident wave power flux, would transfer a power equal to the total transmitted power of the lapped joint into the shadow region. From the figure, it is seen that the transmission cross section peaks sharply at path lengths of approximately 0.45 wavelength and 0.93 wavelength, and more broadly at a path length of 1.45 wavelength. While the exact positions and magnitudes of the sharp peaks are not precisely determined here (because the path length is tested in jumps of 0.05 wavelength, not continuously), parallels with previous work can be discerned. First, the sharp peaks have magnitudes exceeding 10 cells, or 0.25 wavelengths. This is in accordance with results of straight-slot theory [7] which yields a transmission width of $1/\pi$ wavelengths, regardless of the actual slot width, at the slot resonances. Second, the sharp peaks occur at values of path length five to ten percent below integral multiples of one-half wavelength, again in accordance with straight-slot theory [7] for a slot with a gap of 1/40 wavelength.

[6] 160 × 50 cell grid size (using no symmetry), requiring 17 s Cray-2 time.

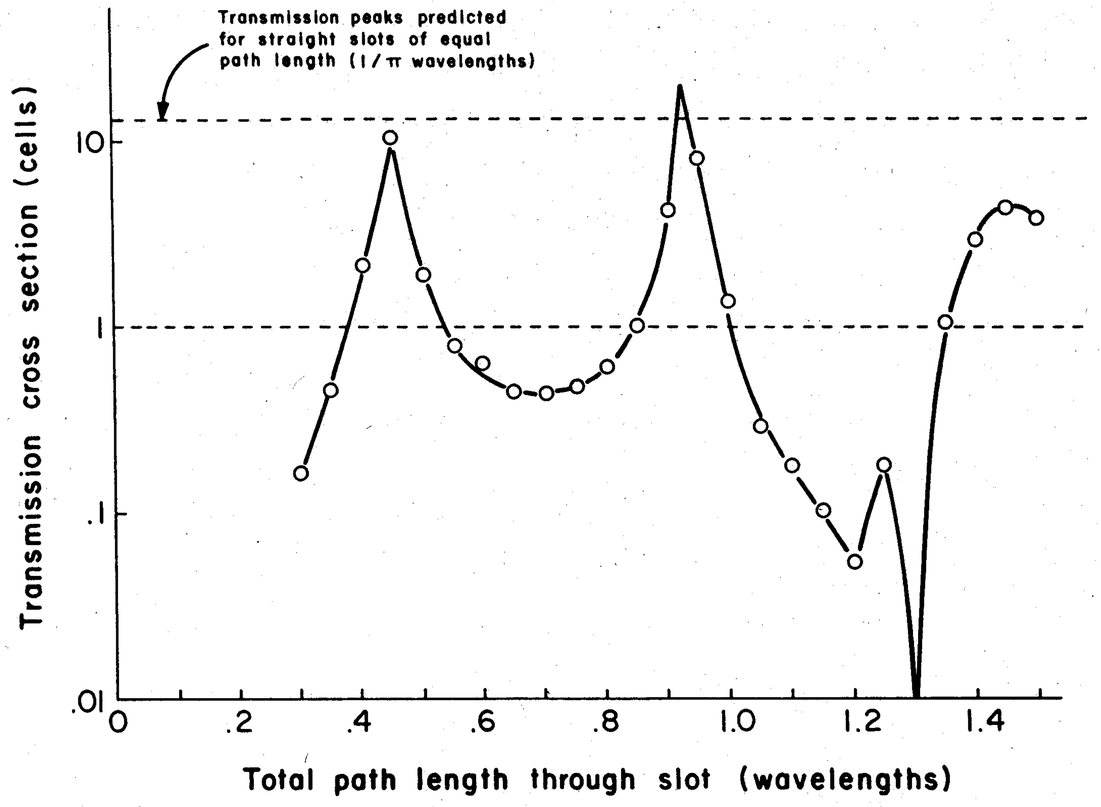

Fig. 11. Transmission cross section of U-shaped lapped joint.

A number of differences, however, exist between the results of Fig. 11 and previous theory. Fig. 11 indicates the possibility of a broad transmission peak (as well as sharp peaks) and distinct structure, including transmission nulls, between the peaks. Previous work for straight slots [7] shows only a single peak-type transmission structure which is repeated without change at half-wavelength intervals of screen depth. One hypothesis for the lapped joint behavior is that, indeed, resonant transmission effects are occurring as the total path length through the joint is varied. In addition, however, the presence of sharply angled turns in the joint path may introduce extra transmission structure due to wave reflections within the joint between the sharply angled turns.

A further indication of a path-length resonance within the lapped joint is found in Figs. 12 and 13. For the case of the total path length equal to 0.45 wavelength (a sharp transmission peak), these figures graph the variation of the gap electric and magnetic fields with position along the joint path. Two types of predictive data for the gap fields are compared: 1) a low-resolution FD-TD model (having 0.09-wavelength cell size), using the contour integral approach to treat the joint gap as 0.28 cell;[7] and 2) the high-resolution FD-TD model (having 0.025-wavelength cell size), previously used in the transmission cross-section study of Fig. 11. The figures show that the magnitude of the gap electric field has almost perfect even symmetry about the midpoint of the joint path, reaching levels of 15 times the incident field near the entry and exit ports A and F. The phase of the gap electric field undergoes a sharp 180° transition at the midpoint of the joint path, where the magnitude has a sharp null. For the gap magnetic field, a spatially broad but intense peak of 15 times the incident field is computed, with even symmetry again exhibited about the midpoint of the joint path.

Figs. 12 and 13 can be interpreted as the field distribution within a kind of one-dimensional resonator, excited very close to resonance, wherein intense electric and magnetic fields are

[7] 50 × 35 cell grid size (using no symmetry), requiring 0.9 seconds Cray-2 time.

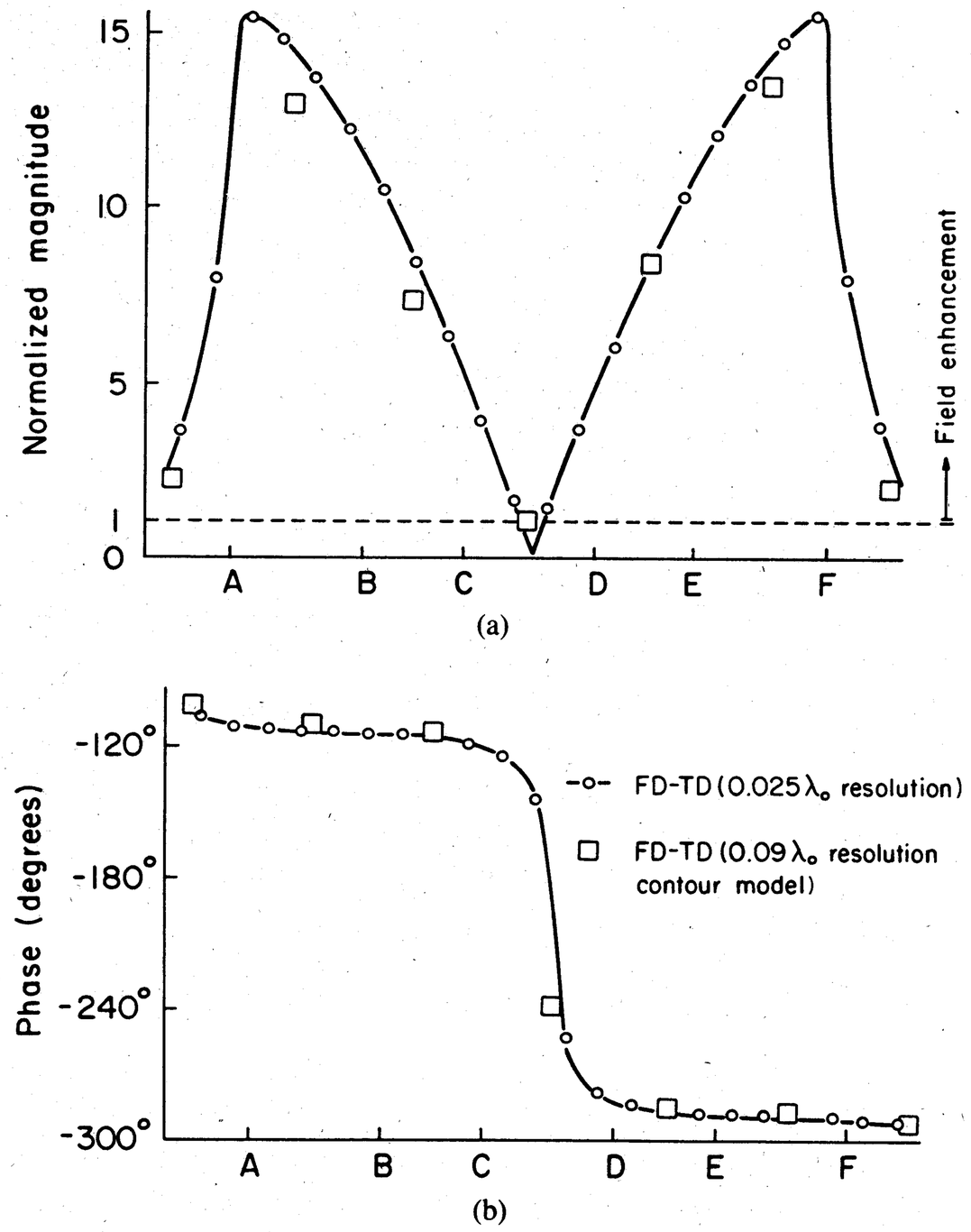

Fig. 12. FD-TD computed electric field within 0.45-wavelength path length, U-shaped lapped joint. (a) $|E_{gap}/E_{inc}|$. (b) $\angle E_{gap}/H_z(A)$.

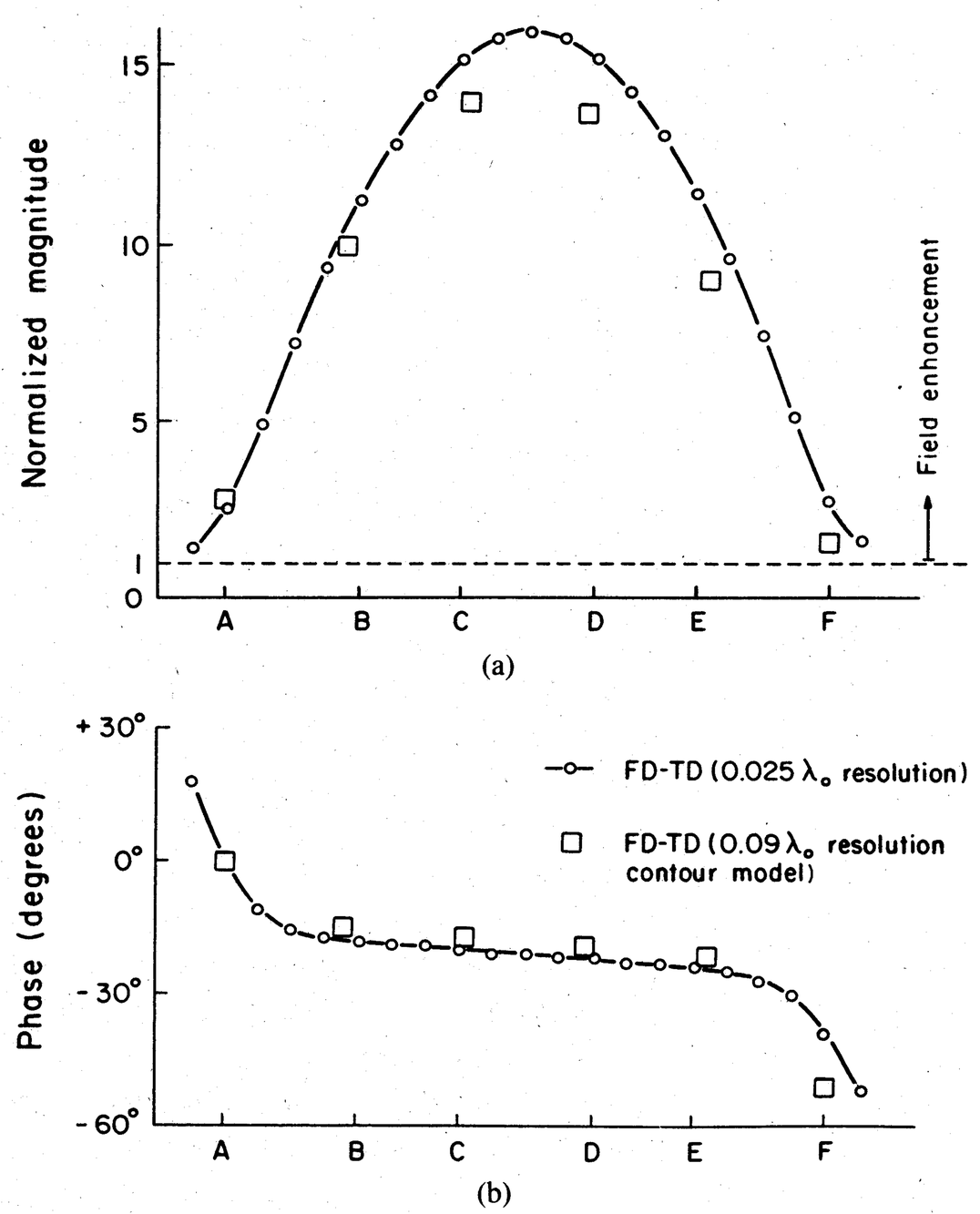

Fig. 13. FD-TD computed magnetic field within 0.45-wavelength path length, U-shaped lapped joint. (a) $|H_{gap}/H_{inc}|$. (b) $\angle H_{gap}/H_z(A)$.

generated in a regular spatial pattern, and energy is interchanged between the electric and magnetic fields with little loss. These figures also provide an intuitive way to understand the enhancement of power transmission through the lapped joint at a path-length resonance. Simply, the very strong peaking of fields within the joint near the output port at F spills over into the shadow region just beyond. Detailed studies of phasing of the "spilled" E and H fields just beyond F show sufficient in-phase components to provide the observed enhancement of transmited power.

Finally, Figs. 12 and 13 indicate a very good level of agreement between the low-resolution and high-resolution FD-TD models, even for a numerically stressful resonant coupling case. This has one major implication, namely, that relatively coarse (1/10 wavelength) FD-TD gridding can be effectively used to model the fine-grained physics of coupling if simple algorithm modifications are made in accordance with the contour integral approach. In this manner, computer resource requirements for using FD-TD models of complex structures can be substantially reduced without sacrificing appreciable accuracy in the modeling results.

V. Summary and Conclusion

This paper has presented a contour integral interpretation for the FD-TD method, which has broad implications for enabling the straightforward modeling of wires, slots, curved surfaces, and other details requiring subcell FD-TD resolution. The contour integral interpretation for FD-TD was first shown to be equivalent to Yee's original formulation [11] for the free-space case. Next, as an example of its utility, the contour approach was used to derive simple (but heretofore not obvious) modifications of the Yee algorithm suitable for modeling thin wires. Using these modifications, FD-TD predictions were then obtained for the azimuthal magnetic field near the surface of an infinitely long wire and a finite-length antiresonant wire for the TM illumination case. Excellent agreement was observed with detailed modal solution and MM numerical benchmark computations.

The paper then focused on its principal topic, detailed FD-TD modeling of electromagnetic wave power transmission through thin straight slots and lapped joints in planar two-dimensional conducting screens of finite width and thickness. The contour approach was used to derive simple (but heretofore not obvious) modifications of the Yee algorithm for screen walls, slot apertures, and slot interiors. Using these modifications, FD-TD predictions were then obtained for the gap electric and magnetic fields in a straight slot. Excellent agreement was observed with a benchmark computation involving a highly resolved MM scattering code. FD-TD modeling was then performed for a lapped joint of variable total path length. The variation of power transmission with total path length was determined to have sharp resonant peaks predicted by previous straight-slot theory [7] but with additional structure attributed to wave reflections internal to the joint. Field peaking of 15:1 was computed within the lapped joint at resonance, with intense gap electric fields appearing near the front and back apertures. A very good level of agreement was found between the low-resolution FD-TD model based on the contour approach, and a high-resolution FD-TD model which served as the benchmark.

It is concluded that the contour integral interpretation for the FD-TD method provides a powerful tool for modeling fine-grained physics of electromagnetic wave coupling. Work reported elsewhere [24] in fact uses this approach to develop accurate models of coupling to wire bundles in a thin-walled cylindrical high-Q metal cavity having a simple slot aperture. Work is ongoing to apply the contour approach to incorporate lapped and threaded (screw-type) joints in such three-dimensional cavity geometries. This will permit exploration of path-length resonant transmission effects and gap field peaking for more realistic models than have yet been attempted.

Acknowledgment

The authors wish to thank Dr. W. Travis White and Dr. Hriar Cabayan of Lawrence Livermore National Laboratory for their technical assistance, encouragement, and support.

References

[1] H. A. Bethe, "Theory of diffraction by small holes," *Phys. Rev.*, vol. 66, pp. 163–182, Oct. 1944.

[2] C. J. Bouwkamp, "On Bethe's theory of diffraction by small holes," *Philips Res. Rep.*, vol. 5, pp. 321–332, Oct. 1950.

[3] C. M. Butler, Y. Rahmat-Samii, and R. Mittra, "Electromagnetic penetration through apertures in conducting surfaces," *IEEE Trans. Antennas Propagat.*, vol. AP-26, pp. 82–93, Jan. 1978.

[4] R. F. Harrington and J. R. Mautz, "A generalized network formulation for aperture problems," *IEEE Trans. Antennas Propagat.*, vol. AP-24, pp. 870–873, Nov. 1976.

[5] D. T. Auckland and R. F. Harrington, "Electromagnetic transmission through a filled slit in a conducting plane of finite thickness, TE case," *IEEE Trans. Microwave Theory Tech.*, vol. MTT-26, pp. 499–505, July 1978.

[6] D. T. Auckland, "Electromagnetic transmission through a filled slit of arbitrary cross section in a conducting plane of finite thickness," Ph.D. dissertation, Syracuse University, Syracuse, NY, June 1979.

[7] R. F. Harrington and D. T. Auckland, "Electromagnetic transmission through narrow slots in thick conducting screens," *IEEE Trans. Antennas Propagat.*, vol. AP-28, pp. 616–622, Sept. 1980.

[8] Y. Leviatan, R. F. Harrington, and J. R. Mautz, "Electromagnetic transmission through apertures in a cavity in a thick conductor," *IEEE Trans. Antennas Propagat.*, vol. AP-30, pp. 1153–1165, Nov. 1982.

[9] R. F. Harrington, *Time-Harmonic Electromagnetic Fields*. New York: McGraw-Hill, 1961.

[10] ——, *Field Computation by Moment Methods*. New York: Macmillan, 1968.

[11] K. S. Yee, "Numerical solution of initial boundary value problems involving Maxwell's equations in isotropic media," *IEEE Trans. Antennas Propagat.*, vol. AP-14, pp. 302–307, May 1966.

[12] A. Taflove and M. E. Brodwin, "Numerical solution of steady-state electromagnetic scattering problems using the time-dependent Maxwell's equations," *IEEE Trans. Microwave Theory Tech.*, vol. MTT-23, pp. 623–630, Aug. 1975.

[13] ——, "Computation of the electromagnetic fields and induced temperatures within a model of the microwave-irradiated human eye," *IEEE Trans. Microwave Theory Tech.*, vol. MTT-23, pp. 888–896, Nov. 1975.

[14] A. Taflove, "Application of the finite-difference time-domain method to sinusoidal steady-state electromagnetic penetration problems," *IEEE Trans. Electromagn. Compat.*, vol. EMC-22, pp. 191–202, Aug. 1980.

[15] A. Taflove and K. R. Umashankar, "A hybrid moment method/finite-difference time-domain approach to electromagnetic coupling and aperture penetration into complex geometries," *IEEE Trans. Antennas Propagat.*, vol. AP-30, pp. 617–627, July 1982.

[16] D. E. Merewether, "Transient currents induced on a body of revolution by an electromagnetic pulse," *IEEE Trans. Electromagn. Compat.*, vol. EMC-13, pp. 41–46, May 1971.

[17] R. Holland, "THREDE: A free-field EMP coupling and scattering

code," *IEEE Trans. Nuc. Sci.*, vol. NS-24, pp. 2416–2421, Dec. 1977.

[18] K. S. Kunz and K. M. Lee, "A three-dimensional finite-difference solution of the external response of an aircraft to a complex transient EM environment: Part I—The method and its implementation," *IEEE Trans. Electromagn. Compat.*, vol. EMC-20, pp. 328–333, May 1978.

[19] B. Engquist and A. Majda, "Radiation boundary conditions for acoustic and elastic wave calculations," *Commun. Pure Appl. Math.*, vol. 32, pp. 313–357, 1979.

[20] G. Mur, "Absorbing boundary conditions for finite-difference approximation of the time-domain electromagnetic field equations," *IEEE Trans. Electromagn. Compat.*, vol. EMC-23, pp. 1073–1077, Nov. 1981.

[21] K. R. Umashankar and A. Taflove, "A novel method to analyze electromagnetic scattering of complex objects," *IEEE Trans. Electromagn. Compat.*, vol. EMC-24, pp. 397–405, Nov. 1982.

[22] A. Taflove and K. R. Umashankar, "Radar cross section of general three-dimensional scatterers," *IEEE Trans. Electromagn. Compat.*, vol. EMC-25, pp. 433–440, Nov. 1983.

[23] A. Taflove, K. R. Umashankar, and T. G. Jurgens, "Validation of FD-TD modeling of the radar cross section of three-dimensional structures spanning up to 9 wavelengths," *IEEE Trans. Antennas Propagat.*, vol. AP-33, pp. 662–666, June 1985.

[24] K. R. Umashankar, A. Taflove, and B. Beker, "Calculation and experimental validation of induced currents on coupled wires in an arbitrary shaped cavity," *IEEE Trans. Antennas Propagat.*, vol. AP-35, pp. 1248–1257, Nov. 1987.

[25] A. Taflove and K. R. Umashankar, "The finite-difference time-domain (FD-TD) method for electromagnetic scattering and interaction problems," *J. Electromagn. Waves Appl.*, vol. 1, pp. 243–267, 1987.

[26] T. G. Jurgens, A. Taflove, and K. R. Umashankar, "Conformal FD-TD modeling of objects with smooth curved surfaces," presented at the National Radio Science Meeting (URSI), Blacksburg, VA, June 1987.

Allen Taflove (M'75–SM'84), for a photograph and biography please see page 766 of the June 1986 issue of this TRANSACTIONS.

Korada R. Umashankar (S'69–M'75–SM'81), for a photograph and biography please see page 765 of the June 1986 issue of this TRANSACTIONS.

Benjamin Beker (S'86), for a photograph and biography please see page 1257 of the November 1987 issue of this TRANSACTIONS.

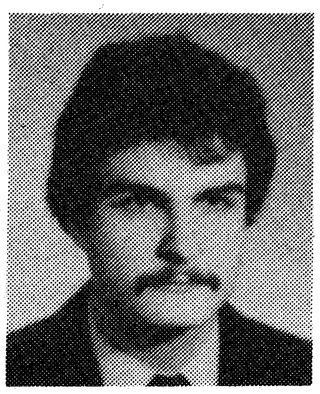

Fady Harfoush (S'86) was born in Beirut, Lebanon, on January 16, 1957. He received the B.S. degree in electrical engineering from Bosphorus University (formerly Robert College), Istanbul, Turkey, in 1981, and the M.S. degree in electrical engineering from Northwestern University, Evanston, IL, in 1984. He is currently working toward the Ph.D. degree at Northwestern University.

His research interests include propagation and scattering of electromagnetic waves using numerical and analytical methods.

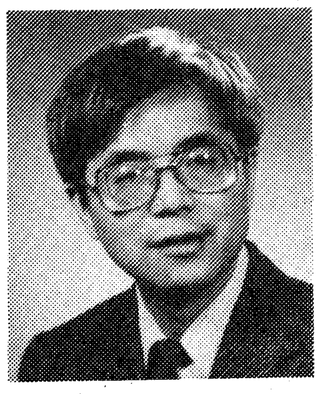

Kane S. Yee received the B.S.E.E., M.S.E.E., and Ph.D. degrees in applied mathematics from the University of California, Berkeley, in 1957, 1958, and 1963, respectively.

From 1959 to 1961, he was employed at Lockheed Missiles and Space Company doing research on high-frequency asymptotic electromagnetic diffractions. From 1964 to 1966, he was employed at Lawrence Livermore National Laboratory to do work on water waves. From 1966 to 1984 he was a Professor of Mathematics and Electrical Engineering at the University of Florida and later at the Kansas State University. He has been a consultant to LLNL since 1966. He rejoined the Lawrence Livermore National Laboratory in 1984. His research areas include electromagnetics, hydrodynamics, and numerical solutions to partial differential equations.

Dr. Yee is the author of the 1966 finite difference time domain electromagnetic numerical algorithm.